COMPUTATIONAL MECHANICS
WCCM VI in conjunction with APCOM '04, *Sept. 5-10, 2004, Beijing, China*

Proceedings of the 6th World Congress on Computational Mechanics, Beijing, China, CD-ROM (2004).

Computation of Cardiovascular Fluid-Structure Interactions with the DSD/SST Method

Ryo Torii[1*], Marie Oshima[1], Toshio Kobayashi[2], Kiyoshi Takagi[3] and Tayfun E. Tezduyar[4]

[1] *Institute of Industrial Science, The University of Tokyo, Komaba 4-6-1, Meguro-ku, Tokyo 153-8505, Japan*
[2] *Japan Automotive Research Institute, Karima 2530, Tsukuba, Ibaraki, 305-0822, Japan*
[3] *School of Medicine, Teikyo University, Kaga 2-11-2, Itabashi-ku, Tokyo, 173-8605, Japan*
[4] *Mechanical Engineering, Rice University-MS321, 6100 Main Street, Houston, TX, 77005, USA*

e-mail:ryota@iis.u-tokyo.ac.jp

Abstract Some cardiovascular diseases, such as atherosclerosis and aneurysm, are believed to depend on hemodynamic factors such as the wall shear stress. Since in vivo measurement techniques are currently unable to resolve phenomena in a living human body, numerical simulations are expected to play an important role in better understanding the relationship between the cardiovascular diseases and hemodynamic factors. We have developed a computational technique for cardiovascular hemodynamic simulations. Patient-specific three-dimensional geometry of an artery can be analyzed. We take into account some of the important factors in human body because we aim to demonstrate in vivo situations in a virtual world. The interaction between the blood flow and the deformation of the arterial walls is a factor that we specifically are focusing on. For such fluid-structure interactions, we have developed a simulation tool based on the DSD/SST method. The simulation tool is applied to a patient-specific model under pulsatile blood flow conditions. The simulations show that the flow field with compliant arterial walls is different from the flow field with rigid arterial walls. Consequently, the distribution of the wall shear stress on the compliant arterial walls is significantly different from that on the rigid arterial walls. We deduce that the compliance of the arterial walls needs to be taken into account in cardiovascular hemodynamic simulations, and the simulation tool we developed can be very effective in investigation of cardiovascular diseases.

Key words: Cardiovascular disease, Fluid-Structure interaction, DSD/SST method

INTRODUCTION

Over 90% of subarachnoid hemorrhages are caused by rupture of cerebral aneurysm, which is shown in Figure 1. Although the risk of rupture is reported to be under 0.1% [1], most aneurysms can be operated on if they are identified. On the other hand, it is also reported in the same paper that the risk of postoperative sequelae is over 10% . Thus it is important to identify aneurysm exposed to high risk of rupture to avoid unnecessary surgical operations. In addition to identification of the risk of individual aneurysms, determining risk factors of rupture of cerebral aneurysms is also necessary to prevent rupture of aneurysms. Because of recent development of medical imaging technique, more aneurysms are identified in physical examinations. Pariculary in Japan, 6% of people have cerebral aneurysm [2], and prediction of rupture of cerebral aneurysm is needed. In previous studies that focused on cerebral aneurysms, the cause of cerebral aneurysms has been thought to be hemodynamic forces, such as the blood pressure and WSS (wall shear stress) [3]. Recently, it was also shown through physiological experiments that some vascular diseases, such as atherosclerosis and aneurysm, are associated with the hemodynamic factors [4]. The authors, therefore, have developed a numerical procedure to investigate mechanisms of cardiovascular diseases. Since in vivo measurement techniques are currently unable to resolve phenomena in a living human body, numerical simulations are expected to play an important role in better understanding the relationship between the cardiovascular diseases and hemodynamic factors.

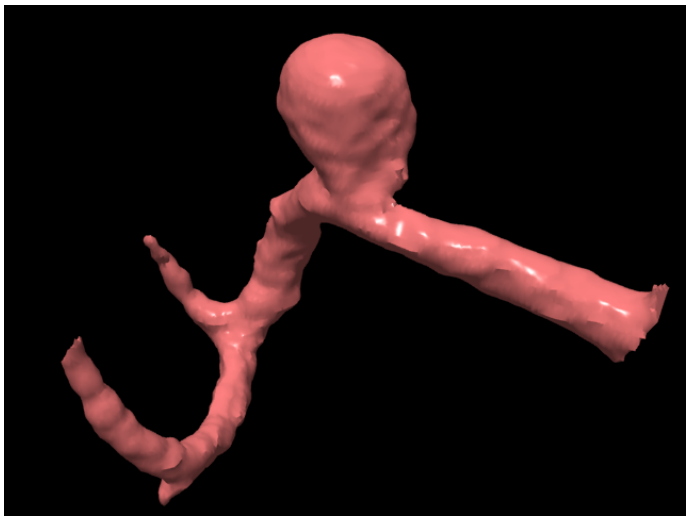

Figure 1: A saccular aneurysm on the middle cerebral artery

In addition to our computational procedure using patient-specific arterial model [5], we take into account some of the important factors in human body because we aim to demonstrate in vivo situations in a virtual world. The interaction between the blood flow and the deformation of the arterial walls is a factor that we are specifically focusing on. For such fluid-structure interactions, we have developed a simulation tool based on the DSD/SST (Deforming-Spatial-Domain / Stabilized Space-Time) method [6, 7, 8]. Although progress of cardiovascular diseases, such as growth of aneurysms, is associated with both mechanical and biological factors, we focus on mechanical factors in this paper. The simulation tool is applied to a patient-specific model, which is one of common aneurysmal site and called the internal carotid artery. A pulsatile flow condition based on measured blood velocity profile is used as boundary condition in the computation. To investigate the interaction between the blood flow and arterial wall motion, the results are compared with those from numerical simulations with rigid arterial walls. We also investigate the effects of elastic arterial walls on blood flow and hemodynamic forces.

NUMERICAL METHODS

In this study the fluid and structural equations are iteratively coupled by force equilibrium at the interface between the fluid and structure. The numerical methods used for fluid mechanics, structural mechanics, and mesh update are described in the following sections.

1 Fluid mechanics

The blood flow is laminar in cerebral arteries [3], and it is governed by the Navier-Stokes equations of incompressible flows:

$$\rho_f \left(\frac{\partial \boldsymbol{u}}{\partial t} + \boldsymbol{u} \cdot \boldsymbol{\nabla} \boldsymbol{u} \right) - \boldsymbol{\nabla} \cdot \boldsymbol{\sigma} = 0, \tag{1}$$

$$\boldsymbol{\nabla} \cdot \boldsymbol{u} = 0, \tag{2}$$

where ρ_f is constant density of fluid and $\boldsymbol{u}$ is the velocity vector. External forces are neglected because we do not consider the effect of external forces, such as gravity or human motion, on the blood flow. Although blood is known as a non-Newtonian fluid, we assume it to be Newtonian in this study. We focus on large arteries with radii of the order 1.0 mm, and both the velocity and shear rate are high in such arteries. The non-Newtonian effects are consequently small enough to be ignored in arteries with large diameters. Then, the stress tensor for a fluid with viscosity μ is described as follows:

$$\boldsymbol{\sigma}(p, \boldsymbol{u}) = -p\boldsymbol{I} + 2\mu\boldsymbol{\varepsilon}(\boldsymbol{u}), \tag{3}$$

where $\boldsymbol{\varepsilon}(\boldsymbol{u})$ is the strain rate tensor :

$$\boldsymbol{\varepsilon}(\boldsymbol{u}) = \frac{1}{2}\left(\boldsymbol{\nabla u} + (\boldsymbol{\nabla u})^T\right). \tag{4}$$

Since our computational method is based on the finite element concept, both the essential and the natural boundary conditions are taken into account as

$$\boldsymbol{u} = \boldsymbol{g} \quad \text{on } (\Gamma)_g, \tag{5}$$

$$\boldsymbol{n}\cdot\boldsymbol{\sigma} = \boldsymbol{h} \quad \text{on } (\Gamma)_h, \tag{6}$$

where $(\Gamma)_g$ and $(\Gamma)_h$ are the complementary subset of the boundary Γ.

Eqs. (1) and (2) are discretized by means of the DSD/SST (Deforming-Spacial-Domain / Stabilized Space-Time) finite element formulation [6, 7, 8]. The DSD/SST method has been applied to a large number of problems with moving boundaries and interfaces, and is well suited to handle the time variant spatial domains. In the formulation, the time interval $(0, T)$ is divided into a sequence of subintervals $I_n = (t_n, t_{n+1})$. A space time domain between Ω_n and Ω_{n+1}, which are spatial domains at the time level t_n and t_{n+1} respectively, is defined as a space-time slab and denoted by Q_n. The space-time boundary of Q_n is denoted by P_n and described by the boundary Γ_t as t traverses I_n. A space-time boundary P_n can be decomposed into $(P_n)_g$ and $(P_n)_h$ with respect to the type of boundary conditions (essential or natural). For each space-time slab, we define the corresponding finite element trial function spaces $(\mathcal{S}^h_{\boldsymbol{u}})_n$ for velocity and $(\mathcal{S}^h_p)_n$ for pressure , and the test function spaces $(\mathcal{V}^h_{\boldsymbol{u}})_n$ and $(\mathcal{V}^h_p)_n = (\mathcal{S}^h_p)_n$. Then, the governing equations are discretized in space and time with finite elements using four dimensional interpolation functions. In this study, we use first-order polynomials in both space and time. Deformation of the computational domain is taken into account as deformation of the integration region. No additional terms are needed for treatment of the moving boundaries. The weak form of the governing equations with the DSD/SST formulation is written as follows: given $(\boldsymbol{u}^h)^-_n$, find $(\boldsymbol{u}^h) \in (\mathcal{S}^h_{\boldsymbol{u}})_n$ and $(p^h) \in (\mathcal{S}^h_p)_n$ such that $\forall \boldsymbol{w}^h \in (\mathcal{V}^h_{\boldsymbol{u}})_n$ and $\forall q^h \in (\mathcal{V}^h_p)_n$:

$$\begin{aligned}
&\int_{Q_n} \boldsymbol{w}^h \cdot \rho_f \left(\frac{\partial \boldsymbol{u}^h}{\partial t} + \boldsymbol{u}^h \cdot \boldsymbol{\nabla u}^h\right) dQ + \int_{Q_n} \boldsymbol{\varepsilon}(\boldsymbol{w}^h) : \boldsymbol{\sigma}(p^h, \boldsymbol{u}^h) dQ \\
&- \int_{(P_n)_h} \boldsymbol{w}^h \cdot \boldsymbol{h} dP + \int_{Q_n} q^h \boldsymbol{\nabla}\cdot \boldsymbol{u}^h dQ + \int_{\Omega} (\boldsymbol{w}^h)^+_n \cdot ((\boldsymbol{u}^h)^+_n - (\boldsymbol{u}^h)^-_n) d\Omega \\
&+ \sum_{e=1}^{(n_{el})_n} \int_{Q^e_n} \frac{1}{\rho_f} \left[\tau_{SUPG}\, \rho_f \left(\frac{\partial \boldsymbol{w}^h}{\partial t} + \boldsymbol{u}^h \cdot \boldsymbol{\nabla w}^h\right) - \tau_{PSPG}\, \nabla \cdot \boldsymbol{\sigma}(q^h, \boldsymbol{w}^h)\right] \\
&\qquad\qquad \cdot \left[\rho_f \left(\frac{\partial \boldsymbol{u}^h}{\partial t} + \boldsymbol{u}^h \cdot \boldsymbol{\nabla u}^h\right) - \nabla \cdot \boldsymbol{\sigma}(p^h, \boldsymbol{u}^h)\right] dQ = 0,
\end{aligned} \tag{7}$$

where the notation $(\cdot)^+_n$ and $(\cdot)^-_n$ denotes the function values at t_n as approached from below and above:

$$(\phi)^{\pm}_n = \lim_{\delta \to 0} \phi|_{t=t_n \pm \delta} \tag{8}$$

The DSD/SST formulation is applied to all space-time slabs $Q_0, Q_1, Q_2, \ldots, Q_{N-2}, Q_{N-1}$, starting with $(\boldsymbol{u})^-_0 = \boldsymbol{u}_0$. In this weak form, the first five integrations represent the Galerkin formulation. The fifth term represents the weak continuity of the velocity in time. The last term is the stabilization based on the SUPG (Streamline-Upwind / Petrov-Galerkin) [9] and PSPG (Pressure-Stabilized / Petrov-Galerkin) [6] formulations. τ_{SUPG} and τ_{PSPG} represent the stabilization parameters. There are a number of ways to define these parameters, and we employ the following definition in this paper:

$$\tau_{SUPG} = \left(\frac{1}{\tau^2_{SUGN12}} + \frac{1}{\tau^2_{SUGN3}}\right)^{-1/2}, \tag{9}$$

$$\tau_{SUGN12} = \left(\sum_{a=1}^{n_{en}} \left|\frac{\partial N_a}{\partial t} + \boldsymbol{u}^h \cdot \boldsymbol{\nabla} N_a\right|\right)^{-1}, \qquad \tau_{SUGN3} = \frac{h^2_{RGN}}{4\nu}, \tag{10}$$

$$h_{RGN} = \left(\sum_{a=1}^{n_{en}} |\boldsymbol{r} \cdot \boldsymbol{\nabla} N_a|\right)^{-1}, \qquad \boldsymbol{r} = \frac{\boldsymbol{\nabla}||\boldsymbol{u}||}{||\boldsymbol{\nabla}||\boldsymbol{u}||\,||}, \tag{11}$$

$$\tau_{PSPG} = \tau_{SUPG}, \tag{12}$$

where N_a is the space-time shape function. For more details on the stabilization parameters, see [10]

2 Structural mechanics

The governing equations for structural mechanics are the equilibrium equations:

$$\rho^s \left(\frac{\partial^2 \boldsymbol{X}}{\partial t^2} - \boldsymbol{f} \right) - \boldsymbol{\nabla} \cdot \boldsymbol{\sigma}^s = 0, \tag{13}$$

where $\boldsymbol{X}$ is the displacement vector, ρ^s is the density of the material, $\boldsymbol{f}$ is the external body forces acting on the structure, and $\boldsymbol{\sigma}^s$ is the Cauchy stress tensor. Although the arterial wall is known to be made of a nonlinear elastic material, we assume it to be made of a linear elastic material in this study. We use a Galerkin finite element formulation and write the weak form as follows:

$$\int_{\Omega_s^0} \rho^s \frac{\partial^2 \boldsymbol{X}}{\partial t^2} \cdot \boldsymbol{w} d\Omega + \int_{\Omega_s^0} \boldsymbol{S} : \delta \boldsymbol{E}(\boldsymbol{w}) d\Omega = \int_{\Gamma_s^t} \boldsymbol{t} \cdot \boldsymbol{w} d\Gamma + \int_{\Omega_s^t} \rho^s \boldsymbol{f} \cdot \boldsymbol{w} d\Omega. \tag{14}$$

The fluid dynamics forces are included in the traction force $\boldsymbol{t}$. Using Newmark-β method [11] for time integration, a nonlinear system of equations is obtained at each time step and can be written in the incremental form as

$$\left(\frac{1}{\beta \Delta t} \boldsymbol{M} + \frac{\gamma}{\beta \Delta t} \boldsymbol{C} + \boldsymbol{K} \right) \Delta \boldsymbol{X}^i = \boldsymbol{R}^i. \tag{15}$$

Here $\boldsymbol{M}$ is the global mass matrix, $\boldsymbol{C}$ is a damping matrix, $\boldsymbol{K}$ is the stiffness matrix, $\boldsymbol{R}^i$ is the residual vector at the ith iteration, $\Delta \boldsymbol{X}^i$ is the ith increment in the nodal displacements vector $\boldsymbol{X}$, and Δt is the time step size. The parameters β and γ control the stability and accuracy of the method. We use $\beta = 0.3225$ and $\gamma = 0.6$ in our study.

3 Mesh update

The fluid mesh is updated by using an automatic mesh update method [12]. In this method the motion of the nodes is governed by the equations of elasticity. The boundary conditions come from the motion of the interface between the fluid and structure.

4 Fluid-structure coupling

The fluid and structural mechanics equations are coupled by a block-iterative coupling method. We define the fluid nodes to be the same as the structural nodes at the interface. Thus information can be directly transferred for each nodal points at the interface. The fluid forces at the interface are treated as external forces on the structure. In return, structural displacements at the interface are treated as essential boundary conditions for the fluid dynamics in the DSD/SST formulation. In iteratively coupled fluid-structure interaction analysis, structural motion might overshoot due to underestimation of the damping effect of the fluid. We perform several iterations within one time step to avoid this problem, which was pointed out in Reference [13].

NUMERICAL EXAMPLES

1 Patient-specific model of intracranial arteries

The authors have developed a numerical simulation procedure based on medical imaging data [5]. In the procedure, three dimensional geometry of artery is extracted from CT (Computed Tomography) using the commercial software ALATOVIEW. A patient-specific geometry of an artery was investigated as numerical example. The model is an artery called the internal carotid artery, which is one of the common sites of cerebral aneurysm. The diameter of the artery is about 4.0 mm. The patient is a male in his 70's. We aim to investigate the interaction between the blood flow and the arterial wall in a steeply curved artery. Both the geometry and mesh configuration of the computational model are shown in Figure 2. The number of fluid and structural nodes are 29,643 and 11,808 respectively. The number of fluid and structural elements are 23,708 and 7,808 respectively. The computational mesh is generated with the commercial software ICEM CFD.

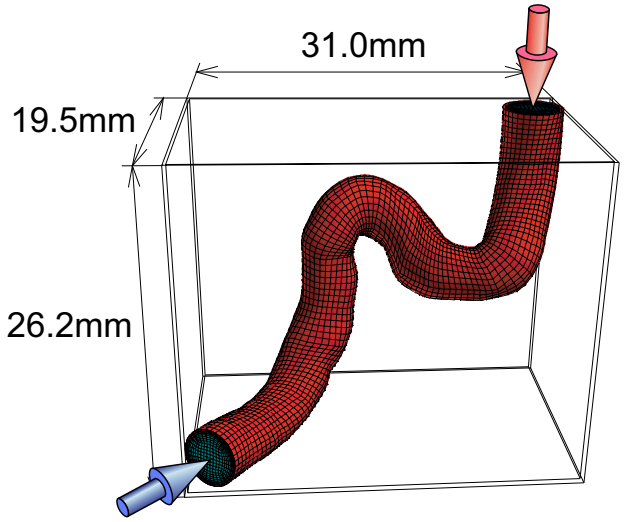

Figure 2: Geometry of the compuational model (blue arrow: inflow, red arrow: pressure resistance of the downstream arterial network)

2 Boundary conditions and initial condition

The inflow boundary condition is a pulsatile velocity profile described with the following Womersley solution of pulsatile flow [14]:

$$w(r,t) = \frac{2B_0}{\pi R^2}\left[1-\left(\frac{r}{R}\right)^2\right] + \sum_{n=1}^{N}\frac{B_n}{\pi R^2}\left[\frac{1-\frac{J_0(\alpha_n \frac{r}{R} i^{3/2})}{J_0(\alpha_n i^{3/2})}}{1-\frac{2J_1(\alpha_n i^{3/2})}{\alpha_n i^{3/2} J_0(\alpha_n i^{3/2})}}\right] e^{in\omega t}, \tag{16}$$

$$Q(t) = \sum_{n=0}^{N} B_n e^{i\omega t}, \tag{17}$$

where r is the cylindrical coordinate and t is time. R denotes the radius of the inlet cross section. J_0 and J_1 are Bessel functions of the first kind of order 0 and 1, respectively. $\alpha_n = R\sqrt{n\omega/\nu}$, where ω is based on one cardiac cycle (=1.0 sec). The non-dimensional parameter $\alpha = R\sqrt{\omega/\nu}$ is known as the Womersley number. B_n are the Fourier coefficients and are determined from the velocity profile measured by ultrasound Doppler velocimetry at the carotid artery of a male in his 20's. The order of series is 20. The pressure resistance due to the downstream arterial network is modeled by the Windkessel model [15] as traction boundary condition of the fluid equations. In Windkessel model of the arterial network, the pressure, flow rate and flow resistance are considered as the voltage, current and resistance in an electric circuit. The pressure is determined by integration of

$$Q = C\frac{dp}{dt} + \frac{p}{R}, \tag{18}$$

where, Q is the flow rate of the arterial system, C is the compliance of the artery, p is the pressure and R is the resistance of the distal arterial network. C and R are determined in an ad hoc fashion to adjust that the pressure ranges from 80 mmHg to 115 mmHg, which is the standard range of blood pressure for a healthy human. The transient behavior of the inflow boundary condition and the downstream resistance are shown in Figure 3. It is shown that the Womersley solution, which is shown with the red line, well describes the measured value, which is shown with the dashed blue line. In the structural calculations, both the upstream and downstream end of the artery is fixed by means of zero-displacement boundary condition. A fully developed flow field with the inflow being the same as the inflow at the beginning of pulsatile boundary condition cycle is applied as the initial condition. The initial displacements and stresses are set to zero for the structure.

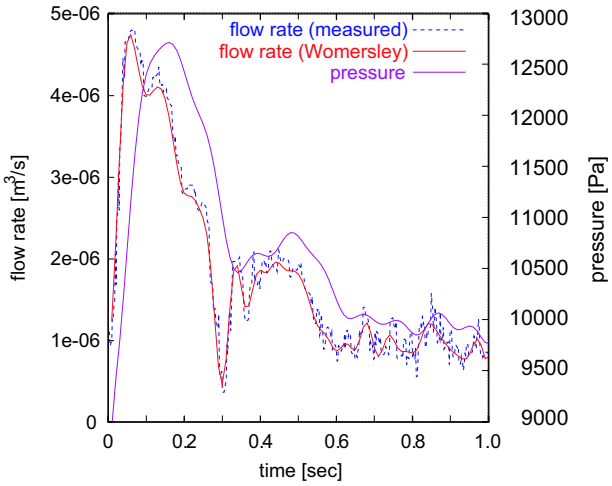

Figure 3: Transient behavior of the boundary conditions

3 Determination of mechanical properties

The blood is assumed to be Newtonian fluid because the apparent viscosity is nearly a constant in arteries with relatively large diameters ($d \sim 5\mathrm{mm}$) [16].

Although the arterial wall is known to be made of a nonlinear elastic material, it is assumed to be made of a linear elastic material in this study. To specify the apparent elastic modulus, we carried out a simple numerical test. We investigated the relationship between the radius and inner pressure of a straight pipe, which is assumed to be the straight portion of an artery. By comparing this to experimental data [17], we specify the elastic modulus E to be 1.0 MPa.

4 Results

Figure 4 shows the deformation of the artery. The transparent geometry shows the initial configuration at the beginning of the systole, and the geometry with the color contours show the configuration at the end of the systole. The color contours depict the magnitude of the displacement. The blood flows from left to right in the figure. Since the artery is fixed at both the downstream and upstream ends of the computational domain, it is reasonable that the maximum displacement is observed in the area between the two ends. The magnitude of the maximum displacement is 0.815 mm, which is 1/5 of the diameter. It is also observed that the displacement of the centerline is larger than the change in the arterial radius. This means that the pulsatile flow does not contribute to the expansion of the artery as much as it contributes to the deformation of the artery as a rigid body motion.

Figures 5 and 6 show the WSS distributions for the elastic and rigid wall models at the end of the systole. The left figures show the distribution from the medial view, and the right figures from the lateral view. The maximum magnitude of the WSS is 139 dym/cm^2 for the elastic wall model and 186 dyn/cm^2 for the rigid wall model. There is not only a quantitative difference between the WSS for the two models, but also a general difference in the WSS distributions. The differences in the location of the concentrated WSS are particularly remarkable because high values of the WSS are believed to affect cardiovascular diseases [4], including cerebral aneurysm. The differences in the overall WSS distributions come from the interaction between the motion of the arterial wall and the blood flow.

Here, we focus on the flow velocity distribution to investigate the reasons behind the differences in the WSS distributions. Figures 7 - 10 show the transient behavior of the velocity distributions for the elastic and rigid wall models. The cross sections A and B are at locations with concentrated WSS (see Figures 5 and 6 for those locations). The systolic period begins at $t = 0.0$ sec, and ends at around $t = 0.8$ sec. Because the Womersley velocity profile at the inlet section is similar to a parabolic profile, relatively parabolic distribution of the velocity can be seen at the cross section A at $t = 0.01$ sec. The area of high velocity magnitude takes a crescent-like shape and approaches the arterial wall. This yields high velocity magnitude near the wall, resulting in high WSS at the wall. Comparing Figures 7 and 8, it is observed that

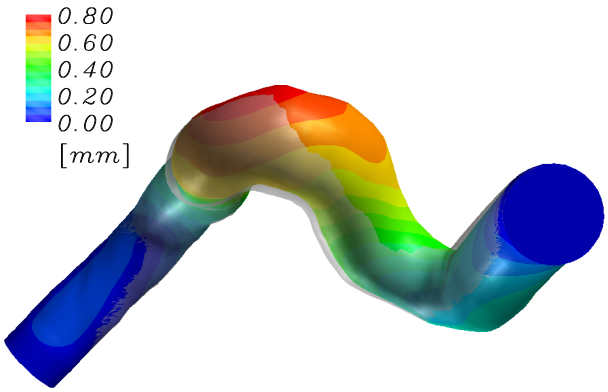

Figure 4: Deformation of the artery at the end of a systole (color contours describe the magnitude of the displacement, with the transparent geometry showing the configuration at the beginning of the systole)

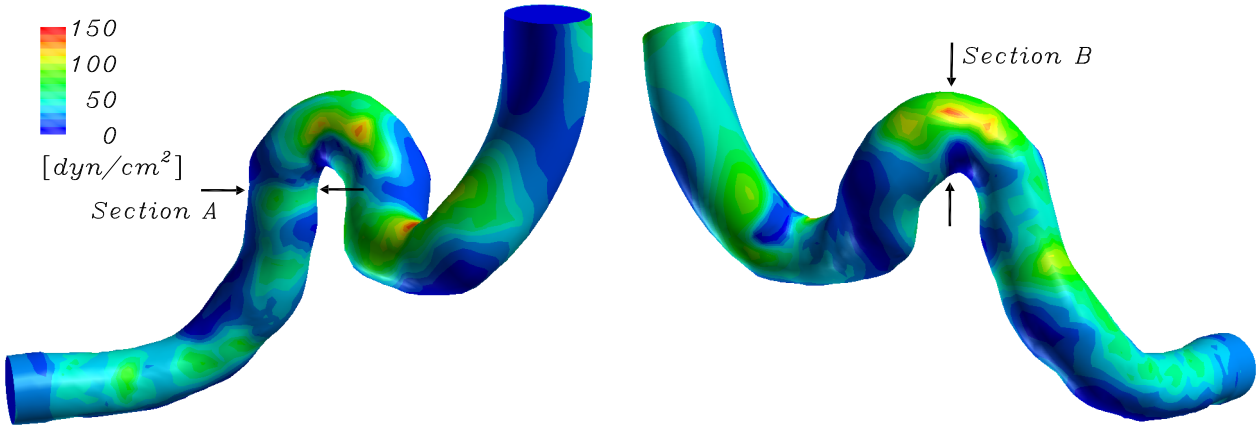

(a) medial view (b) lateral view

Figure 5: WSS distribution with elastic wall model

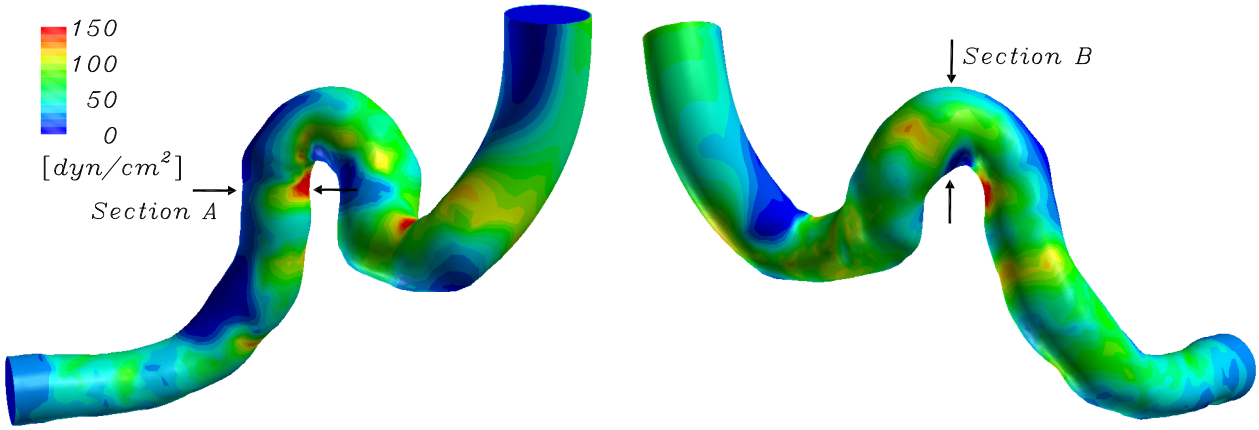

(a) medial view (b) lateral view

Figure 6: WSS distribution with rigid wall model

the magnitude and gradient of the velocity near the wall, especially around the area indicated by the black arrow in Figure 7, are significantly smaller for the elastic wall model. When the deformation of the arterial wall is taken into account, the cross sectional area is enlarged by the systolic increase of the pressure, and the mean velocity magnitude, therefore, decreases. In this result, the area of the cross section A for the elastic wall model is 6% larger than it is for the rigid wall model. In addition to the expansion of the cross sectional area, the motion of the entire cross section A towards the top of the figure moves the arterial wall away from the area of high velocity magnitude. This is the reason why the magnitude of the WSS in the elastic wall model is smaller than it is in the rigid wall model around the cross section A. On the other hand, the magnitude of the WSS in the elastic wall model is larger than it is in the rigid wall model around the cross section B. Although the velocity distributions are similar in both models at the beginning of the systolic period, the locations of the areas with high velocity magnitude are different at the end of the systole. The magnitude of the velocity gradient is larger in the rigid wall model around the area indicated by the black arrow in Figure 9. The magnitude of the WSS around this area in the elastic wall model is consequently larger than it is in the rigid wall model.

The results shown here indicate that computation of the WSS in estimating the risk of cardiovascular disease is significantly affected by the motion of the arterial wall. Therefore we believe that fluid-structure interactions play a critical role in investigation of cardiovascular diseases.

CONCLUSIONS

A numerical procedure for investigating the blood flow and arterial wall interactions is developed based on the DSD/SST method. The procedure is applied to a patient-specific model of the cerebral artery. The results show that the WSS distributions are affected by the arterial wall deformations. Since the WSS distribution is key to investigation of cardiovascular diseases, the results show that computational procedure developed in this paper can be an effective tool to conduct hemodynamic studies of cardiovascular diseases. The results also indicate the importance of the wall deformation in this kind of studies.

Acknowledgements

A part of this research was done in “Frontier Simulation Software for Industrial Science (FSIS)” project supported by IT program of Ministry of Edcation, Culture, Sports, Sceince and Technology (MEXT). Authors also acknowledge Dr. Motoaki Hayakawa, Fujita health university, for contribution of CT data and acknowledge Toshiba Medical, Inc. for contribution of the software “ALATOVIEW”.

References

[1] The International Study of Unruptured Intracranial Aneurysms Investigators. Unruptured intracranial aneurysms - risk of rupture and risks of surgical intervention. *The New England Journal of Medicine*, 339(24):1725–1733, 1998.

[2] T. Nakagawa and K. Hayashi. The incidence and treatment of asymptomatic, unruptured cerebral aneurysms. *Journal of Neurosurgery*, 80:217–223, 1994.

[3] T. Karino, S. Takeuchi, N. Kobayashi, M. Motomiya, and S. Mabuchi. Fluid dynamics of cerebrovascular disease (in Japanese). *Neurosurgeons*, 12:15–24, 1993.

[4] A. M. Malek, S. L. Alper, and S. Izumo. Hemodynamic shear stress and its role in atherosclerosis. *The Journal of the American Medical Association*, 282:2035–2042, 1999.

[5] R. Torii, M. Oshima, T. Kobayashi, and K. Takagi. The hemodynamic study of the cerebral artery using numerical simulations based on medical imaging data. *Journal of Visualization*, 4(3):277–284, 2001.

[6] T. E. Tezduyar. Stabilized finite element formulations for incompressible flow computations. *Advances in Applied Mechanics*, 28:300–312, 1991. ← 1992

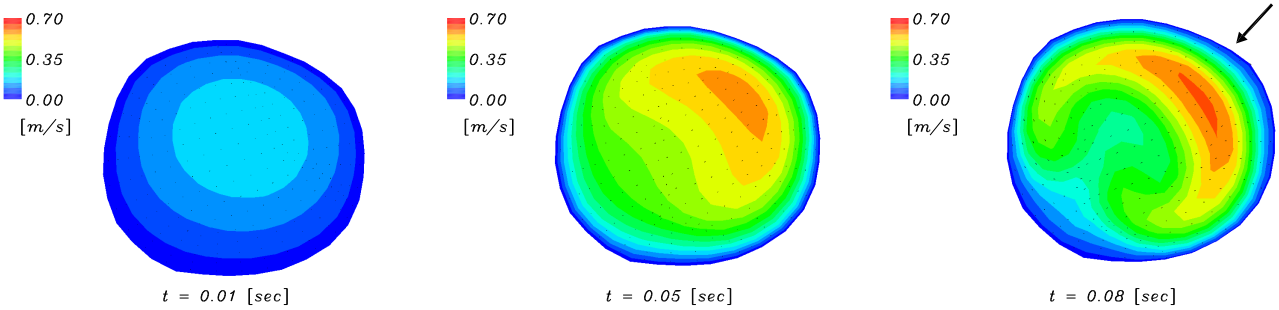

Figure 7: Transient behavior of the flow velocity distribution in the cross section A for the elastic wall model

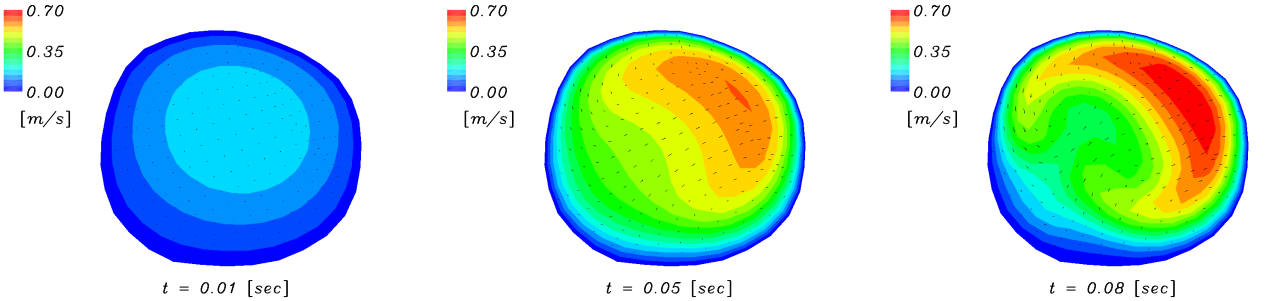

Figure 8: Transient behavior of the flow velocity distribution in the cross section A for the rigid wall model

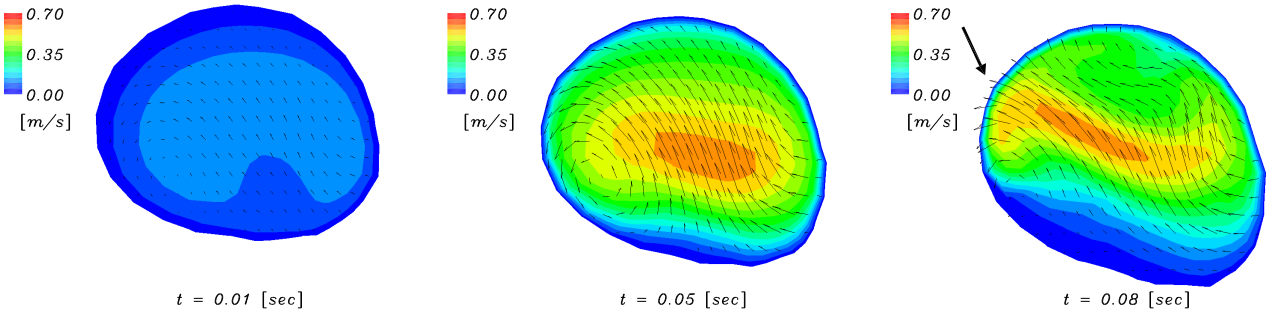

Figure 9: Transient behavior of the flow velocity distribution in the cross section B for the elastic wall model

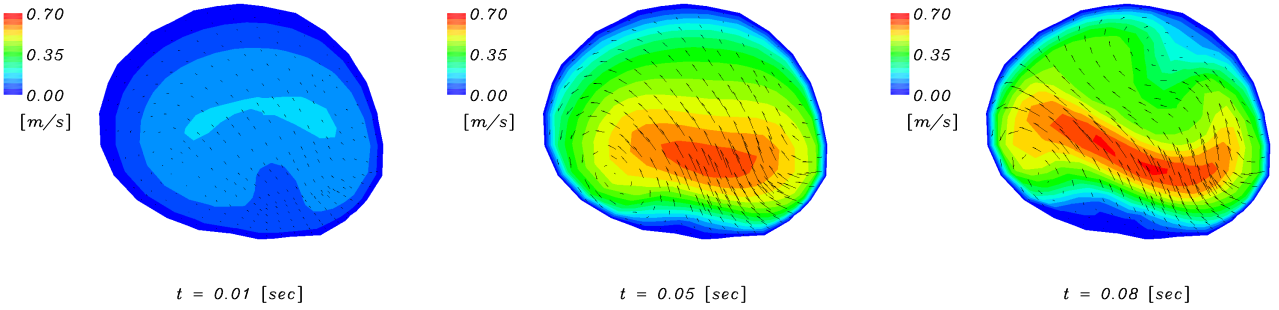

Figure 10: Transient behavior of the flow velocity distribution in the cross section B for the rigid wall model

[7] T. E. Tezduyar, M. Behr, and J. Liou. A new strategy for finite element computations involving moving boundaries and interfaces - The deforming-spatial-domain/space-time procedure: I. The concept and the preliminary numerical tests. *Computer Methods in Applied Mechanics and Engineering*, 94:339–351, 1992.

[8] T. E. Tezduyar, M. Behr, S. Mittal, and J. Liou. A new strategy for finite element computations involving moving boundaries and interfaces - The deforming-spatial-domain/space-time procedure: II. Computation of free-surface flows, two-liquid flows, and flows with drifting cylinders. *Computer Methods in Applied Mechanics and Engineering*, 94:353–371, 1992.

[9] A. N. Brooks and T. J. R. Hughes. Streamline upwind/Petrov-Galerkin formulations for convection dominated flows with particular emphasis on the incompressible navier-stokes equations. *Computer Methods in Applied Mechanics and Engineering*, 32:199–259, 1982.

[10] T.E. Tezduyar. Computation of moving boundaries and interfaces and stabilization parameters. *International Journal for Numerical Methods in Fluids*, 43:555–575, 2003.

[11] N. M. Newmark. A method of computation for structural dynamics. *A.S.C.E. Journal of Engineering Mechanics*, 85:67–94, 1959.

[12] T.E. Tezduyar, M. Behr, S. Mittal, and A.A. Johnson. Computation of unsteady incompressible flows with the stabilized finite element methods–space-time formulations, iterative strategies and massively parallel implementations. *New Methods in Transient Analysis*, PVP-246/AMD-143:7–24, 1992.

[13] T. Nomura. ALE finite element computations of fluid-structure interaction problems. *Computer Methods in Applied Mechanics and Engineering*, 112:291–308, 1994.

[14] J. R. Womersley. Method for the calculation of velocity, rate of flow and viscos drag in arteries when the pressure gradient is known. *Journal of Physiology*, 127:553–563, 1955.

[15] F. Otto. Die grundform des arteriellen pulses. *Zeitung fur Biologie*, 37:483–586, 1899.

[16] D. A. McDonald. *Blood flow in arteries*. Edward Arnold, 2nd edition, 1974.

[17] K. Hayashi, H. Handa, S. Nagasawa, A. Okumura, and K. Moritake. Stiffness and elastic behavior of human intracranial and extracranial arteries. *Journal of Biomechanics*, 13:175–184, 1980.